AIP | Physics of Fluids

Hydrodynamic interactions of two nearly touching Brownian spheres in a stiff potential: Effect of fluid inertia

Milad Radiom, Brian Robbins, Mark Paul, and William Ducker

Citation: Physics of Fluids **27**, 022002 (2015); doi: 10.1063/1.4908295
View online: http://dx.doi.org/10.1063/1.4908295
View Table of Contents: http://scitation.aip.org/content/aip/journal/pof2/27/2?ver=pdfcov
Published by the AIP Publishing

PHYSICS OF FLUIDS **27**, 022002 (2015)

Hydrodynamic interactions of two nearly touching Brownian spheres in a stiff potential: Effect of fluid inertia

Milad Radiom,[1,a)] Brian Robbins,[2] Mark Paul,[2] and William Ducker[1,b)]
[1]*Department of Chemical Engineering, Virginia Tech, Blacksburg, Virginia 24060, USA*
[2]*Department of Mechanical Engineering, Virginia Tech, Blacksburg, Virginia 24060, USA*

(Received 13 March 2014; accepted 2 February 2015; published online 26 February 2015)

The hydrodynamic interaction of two closely spaced micron-scale spheres undergoing Brownian motion was measured as a function of their separation. Each sphere was attached to the distal end of a different atomic force microscopy cantilever, placing each sphere in a stiff one-dimensional potential (0.08 Nm^{-1}) with a high frequency of thermal oscillations (resonance at 4 kHz). As a result, the sphere's inertial and restoring forces were significant when compared to the force due to viscous drag. We explored interparticle gap regions where there was overlap between the two Stokes layers surrounding each sphere. Our experimental measurements are the first of their kind in this parameter regime. The high frequency of oscillation of the spheres means that an analysis of the fluid dynamics would include the effects of fluid inertia, as described by the unsteady Stokes equation. However, we find that, for interparticle separations less than twice the thickness of the wake of the unsteady viscous boundary layer (the Stokes layer), the hydrodynamic interaction between the Brownian particles is well-approximated by analytical expressions that neglect the inertia of the fluid. This is because elevated frictional forces at narrow gaps dominate fluid inertial effects. The significance is that interparticle collisions and concentrated suspensions at this condition can be modeled without the need to incorporate fluid inertia. We suggest a way to predict when fluid inertial effects can be ignored by including the gap-width dependence into the frequency number. We also show that low frequency number analysis can be used to determine the microrheology of mixtures at interfaces. [http://dx.doi.org/10.1063/1.4908295]

INTRODUCTION

Particles are found in a wide-range of natural and artificial materials such as blood, milk, paint, mud, and soil, so the flow of particulate materials has long been of interest. The fluid flow near and in the far field of a single particle has been studied by Stokes and Boussinesq (1903).[1–4] The hydrodynamic interaction between two particles has also received considerable attention.[5–9] In colloidal suspensions, the particles are normally Brownian. For large particles (~1 μm), the amplitude of their (thermal) oscillations is much smaller than the size of the particle (see below). This length scale difference results in specific interactions between Brownian particles and thus many experiments have been performed on hydrodynamic interactions between Brownian particles for interparticle separations no less than about 1 μm using optical tweezers (OT).[10–12]

The purpose of this paper is to examine the hydrodynamic interaction between two Brownian particles at small separations and when the frequency of thermal oscillations is high (resonance frequency at 4 kHz in this study). An example of a high frequency technology is the electroacoustic determination of the zeta potential and the particle size,[13] where particles are oscillated using a high frequency electric field or acoustic field. A full account of particle size and surface potential in this

a)milad.radiom@unige.ch
b)wducker@vt.edu

situation requires an understanding of the interparticle hydrodynamic and electrical interactions. Another example is fast microrheology where neglecting to include the unsteady inertial effects at very short time scales results in errors in fluid characterization.[11,14]

Previous theoretical study of the hydrodynamic interactions between two Brownian spheres shows that, at high frequency and at small[9] or large[7–9] separations, the fluid inertia becomes comparable to or even larger than the viscous forces. In this work, our criterion for small separations is when the ratio of the gap width to the thickness of the wake of the unsteady viscous boundary layer (Stokes layer) is small. The Stokes layer is of order $\delta_s = \sqrt{2\upsilon/\omega}$, where υ is the kinematic viscosity and ω is the oscillation frequency in rad^{-1}. For high oscillation frequency and small interparticle separations, Hinch and Nitsche[9] found that the oscillation frequency (or the fluid inertia) plays an important part in the interaction force between the spheres while the spheres are kept at constant distance with overlapping Stokes layers and the frequency is varied. However, in this paper, we show that, at small separations, the hydrodynamic coupling between the spheres is accurately predicted by a low frequency approximation. Under these conditions, the interaction force depends on the separation between the particles, and not the frequency.

The fluid motion surrounding an oscillating particle obeys the Navier-Stokes equation[2,15,16]

$$-i\omega \mathrm{Re}_\omega \,\vec{\hat{u}} + \mathrm{Re}\,\vec{\hat{u}}.\vec{\nabla}\vec{\hat{u}} = -\vec{\nabla}\hat{p} + \nabla^2\vec{\hat{u}} \tag{1}$$

with the no-slip boundary condition on the surface of the particle. In Eq. (1), $\hat{}$ denotes Fourier transformed parameter, $\vec{\hat{u}}$ is the velocity field, and $\hat{p}$ is the pressure field. The Reynolds number is defined by $\mathrm{Re} \equiv UL/\upsilon$ and the frequency number is defined by $\mathrm{Re}_\omega \equiv L^2/T_o\upsilon$, where U and T_o are the characteristic velocity and time scale of particle motion in an otherwise stationary background fluid, and L is the characteristic length. For most practical applications (e.g., the stability of colloidal solutions), Re and $\mathrm{Re}_\omega < O(1)$ and thus the majority of experimental and theoretical works have focused on the non-inertial form of Eq. (1)[12,17–21]

$$0 = -\vec{\nabla}\hat{p} + \nabla^2\vec{\hat{u}}. \tag{2}$$

For Brownian particles in a potential field with stiffness k, the root mean squared (rms) velocity of thermal oscillation is $U = A\omega_o$ where from the equipartition theorem, $A = \sqrt{k_B T/k}$ is the rms amplitude of thermal oscillation and $\omega_o = 2\pi/T_o$ is the resonance frequency of oscillation. k_B is the Boltzmann's constant and T is the absolute temperature. For A much smaller than the characteristic length L, $\mathrm{Re}_\omega \gg \mathrm{Re}$,[3,9] which results in the unsteady Stokes equation[15]

$$-i\omega \mathrm{Re}_\omega \,\vec{\hat{u}} = -\vec{\nabla}\hat{p} + \nabla^2\vec{\hat{u}}. \tag{3}$$

The relative importance of the unsteady term $(-i\omega \mathrm{Re}_\omega \,\vec{\hat{u}})$ is determined by the frequency number Re_ω. For fluid flow around a *single particle*, the particle radius is the normal choice for the characteristic length L. For the hydrodynamic interaction between *two particles*, the gap width between the particles becomes important: thus, there is an outer flow field of each sphere with the bulk fluid and a flow field in the gap of the two particles where there is hydrodynamic interaction. We suggest that for the hydrodynamic interaction the relevant characteristic length is half the gap width between the particles ($\frac{1}{2}D$) (see Figure 1).

It is known that the friction coefficient of an oscillating sphere, ζ_{sph}, depends on the frequency of oscillation (see Eq. (4)).[1] The oscillation of the sphere results in an unsteady viscous boundary layer with depth ξ_v around it.[10] The wake of this viscous layer has a penetration depth of order $\delta_s = \sqrt{2\upsilon/\omega}$.[3] ξ_v is about $4\delta_s$ for a sphere.[10,11] Comparing δ_s to the radius of the particle a, two limiting cases are identified for the fluid motion around a single particle in which case $L = a$. One limiting case occurs when $\delta_s >> a$. This can occur for low frequencies of oscillation where $\mathrm{Re}_\omega\left(= 2a^2/\delta_s^2\right) << 1$. In this case, the drag on the single sphere is given by Stokes' formula $6\pi\eta a$, where η is the fluid dynamic viscosity. The other limiting case occurs at high frequencies where $\delta_s \le a$ and $\mathrm{Re}_\omega \ge 1$. In this case, the drag on the sphere increases to[1,3]

$$\zeta_{sph} = 6\pi\eta a\,(1 + a/\delta_s)\,. \tag{4}$$

By introducing a new length scale for the interparticle hydrodynamic interaction, i.e., $L = \frac{1}{2}D$, a new frequency number is introduced, $\mathrm{Re}_{\omega,g} = \frac{1}{2}D^2/\delta_s^2$ (where g denotes the gap region), and it

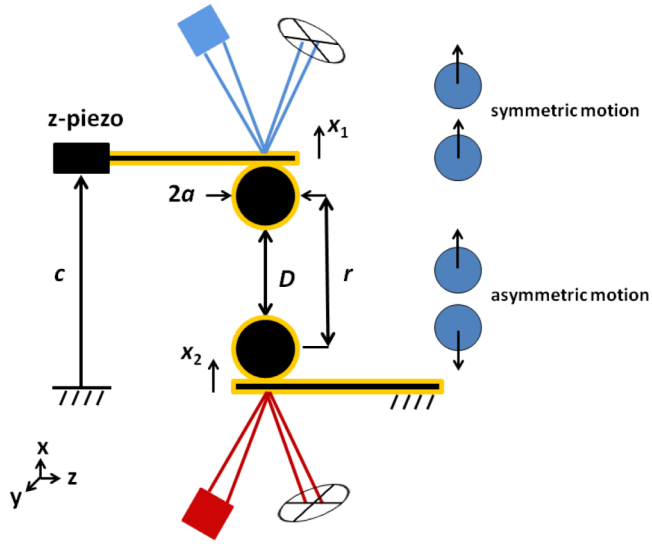

FIG. 1. Schematic of the experiment. a is the radius of a sphere, c is the distance travelled by the piezoelectric drive, D is the separation between the two spheres, and $r = D + 2a$ is the center-to-center distance. The dimensionless center-to-center distance is $\rho = r/a$. x_1 and x_2 are the thermally stimulated deflections of the cantilever-sphere assemblies that are detected by individual detection systems. The z-piezo in the top assembly is part of the commercial AFM and is used to vary the separation between the two spheres. In symmetric motion, the spheres move in the same direction while in asymmetric motion, they move in opposite directions.

should be possible for the fluid inertial forces to be important for a single particle but not for a pair of particles (i.e., where $D \le \delta_s \le a$). An atomic force microscopy (AFM) experiment, with its control of interparticle separation, allows us to examine both the single-particle and the two-particle regimes for the same particle. The purpose of the current paper is to use such measurements to understand the effect of fluid inertia for the two-particle case. For the experiments described in this paper, the resonance frequency was about 4 kHz and we calculate the frequency number at this 4 kHz. However, because of damping, the high amplitudes of Brownian motion are spread over the range 1–9 kHz, so that there is a range of frequency numbers in all experiments. The depth of the wake of unsteady viscous boundary layer is $\delta_s = 9$ μm (calculated at 4 kHz). The particle radius is $a = 15$ μm (unless otherwise stated). The gap of the two particles D is varied from a few nanometers (nearly touching) to a few micrometers. Although in our experiments the *single* particle-fluid interaction has a high frequency number $\mathrm{Re}_\omega = 2a^2/\delta_s^2$ ($\mathrm{Re}_\omega = 6$), the *two* particle interaction will have a low frequency number ($\mathrm{Re}_{\omega,g} \le 1$) for $D \le \sqrt{2}\delta_s$ if we use the characteristic length $\frac{1}{2}D$ in the definition of the frequency number for fluid motion in the gap of the two spheres. It is thus interesting to see whether the experimental interparticle hydrodynamic interaction can be accurately modeled with non-inertial formulae (Eq. (2))[5,6] even when a single particle is at high frequency number.

For the hydrodynamic interaction between *two* spheres, OT has proven to be a valuable technique. Optical tweezers use a laser beam to exert a potential with a stiffness of about 10^{-6}–10^{-5} N m^{-1}, that is about 10^4 softer than an AFM cantilever and usually results in an overdamped oscillator. Recently, Atakhorrami *et al.*[10,11] explored the unsteadiness of interparticle hydrodynamic interactions by pushing the time resolution of OT measurements to the μs range. Neglecting particle inertia[22] and the restoring force due to the soft harmonic potential applied by laser beams, the fluid velocity field was related to the drag force via $\vec{\hat{u}} = -i\omega\alpha\vec{\hat{F}}$, where α is the interparticle hydrodynamic complex response function and $\vec{\hat{F}}$ is the force exerted by the particle on the fluid.[23] In applications such as OT (i.e., highly overdamped oscillators), the power spectral density of the cross-correlation of thermal fluctuations of the two spheres

$$G_{12} = \int \langle x_1(t)\, x_2(0)\rangle\, e^{i\omega t} dt, \tag{5}$$

can be related to the imaginary part of the complex response function, α'', via the fluctuation-dissipation theorem[11,22]

$$G_{12}(r,\omega) = \frac{4k_BT}{\omega}\alpha''(r,\omega), \tag{6}$$

where x_1 and x_2 are the thermal fluctuations of the position of the two spheres and r is the center-to-center distance. For motion parallel (||) to the centerline of the two spheres α'' is[11]

$$\alpha''_{||}(r,\omega) = \frac{1}{4\pi\eta r\omega} Z, \tag{7}$$

where $(4\pi\eta r\omega)^{-1}$ is the steady interparticle hydrodynamic response function, known as Oseen's response, and Z is a correction due to unsteady fluid inertia[10,11]

$$Z = \frac{[(1+z)\sin z - z\cos z]\, e^{-z}}{z^2}, \tag{8}$$

where $z = r/\delta_s$.

In optical tweezers, the small restoring force and small particle inertia[22] make it possible to relate G_{12} to α'' via Eq. (6). Note that the effective particle inertia is not only due to particle mass but also due to the mass of the fluid displaced.[1] The displaced fluid mass is frequency dependent and is given by $\frac{4}{3}\pi\rho_f a^3\left(\frac{1}{2} + \frac{9\delta_s}{4a}\right)$, where ρ_f is the fluid density. The fluid loaded mass (mass of the sphere plus the mass of the displaced fluid) is then

$$m_{\text{sph}} = \left(\rho_{\text{sph}} + \rho_f\left(\frac{1}{2} + \frac{9\delta_s}{4a}\right)\right)\frac{4}{3}\pi a^3, \tag{9}$$

where ρ_{sph} is the density of the sphere and $\frac{4}{3}\pi\rho_{\text{sph}}a^3$ is the mass of sphere. We note the distinction between the fluid inertia ($-i\omega \text{Re}_\omega\, \vec{\hat{u}}$ term in Eq. (3)) and the inertia of the particle (Eq. (9)). The governing equation for the fluid is the Navier-Stokes equation and fluid inertia becomes significant at high Re_ω, while significant particle inertia appears in the correlation function between the two closely spaced spheres (Eqs. (11)–(17)). The frequency dependent drag (Eq. (4)) and mass (Eq. (9)) restrict the permissible frequencies for the accurate application of Eq. (6). For high frequency measurements (~100 kHz), one has to choose small particles on the order 1 μm in radius. The stiffness of the external potential should be kept very small $k < 0.02$ N m^{-1}, while for stiffer potentials Eq. (6) fails for any size of the microparticle. One shortcoming of optical tweezers is that the smallest interparticle separation is usually more than twice the wavelength of the laser beam (~1000 nm),[12,18] so near-touching interparticle separations are inaccessible, which excludes interparticle collisions, where lubrication forces are greatest. This regime is important for interactions in concentrated suspensions, and during the collisions between particles that determine colloidal stability.

Our approach has many similarities with the OT technique, but instead of applying the external potential using laser beams, we apply the potential by attaching an AFM cantilever to each particle in a device that we call correlation force spectrometer (CFS).[24–26] The cantilevers apply a relatively stiff external potential (0.08 N m^{-1}) in one direction (along the x direction in Figure 1), and much stiffer potentials in the other directions (perpendicular to x and torsional). This restricts the Brownian motion to be most significant in one direction and parallel to the centerline of the spheres. The potential force exerted by AFM cantilevers is known to be harmonic, $F_{ext} = -kx$, where x is the deflection from the equilibrium position. The particle inertia, as well as the restoring force, is important in our experiments and is included in the cross-correlation function analysis (Eqs. (11)–(17)) for a more accurate measurement of the hydrodynamic interaction.

In our experiments, δ_s is fixed while r (see Figure 1) is varied from the sum of the particles' radii (near collision) to a few micrometers. We compared our experimentally calculated interparticle hydrodynamic interaction with available theories that were developed for the hydrodynamic interaction between two spheres at low Reynolds and frequency numbers.[5,6] Our experimental data

are in good agreement with these theories at near touching separations to about $2\delta_s$ (the maximum separation we measured), which supports our choice of characteristic length for inner flow region described above. We show that the unsteady fluid inertial effects are unimportant for interparticle separation D less than about $2\delta_s$. We attribute this effect to the overlapping δ_s surrounding each sphere. The underlying physics is that the elevated frictional forces at narrow gaps dominate fluid inertial effects. Therefore, we use the ratio of the separation between particles D to δ_s to determine when the unsteady inertial effects are unimportant for interparticle interactions. This ratio is independent of the size of particles.

MATERIALS AND METHODS

Figure 1 shows a schematic of the experiment, which is the same as described in Ref. 24, except that in the current work, there is a sphere attached to the unclamped end of each cantilever. Each microsphere, 30 μm or 100 μm-diameter (borosilicate glass, Duke Standards), was glued (epoxy) to the distal end of a different AFM cantilever, $200 \times 20 \times 1$ μm^3 (ORC8-D, Bruker, Inc.). The experiments were performed in deionized water and at room temperature 22 °C. In experiments on nanoparticle solutions, we used Ludox TMA colloidal silica suspensions (22 nm diameter) in deionized water (34 wt %, sigma-Aldrich, St. Louis, MO, USA). 6% and 8% nanoparticle solutions were prepared by adding deionized water that was purified in a Barnstead EASYpure II (Thermo Fisher Scientific, Inc., Asheville, NC, USA). To significantly reduce the ion concentration in the dilute solutions, an ion-exchange resin (AG 501-X8, Bio-Rad Laboratories, Hercules, CA, USA) was added, and the solution bottles were placed on a vertical rotator overnight. Solutions of 0.5M NaOH (Sigma-Aldrich) and 0.5M NaCl (Sigma-Aldrich) were prepared and used to adjust the pH to 7 and ionic strength to the range 1 to 5 mM.

The spring constants of each cantilever were determined using the thermal noise method, which has an uncertainty of about 15%-20%[27] which propagates directly into uncertainty in ζ_{ij} (see Eq. (11)). The deflections of each of the cantilever-sphere assemblies, $x_1(t)$ and $x_2(t)$, were measured using the optical lever technique[28] with a separate laser and photodiode for each assembly. The top detection system was part of a commercial AFM (MFP3D-Bio, Asylum Research, Oxford Instruments), which includes a superluminescent laser diode with an 860 nm wavelength. The customized bottom detection system includes a laser with a 680 nm wavelength (51nanoFCM, Schäfter + Kirchhoff GmbH) and a photosensitive diode (QP50-6-18u-SD2, Pacic Silicon Sensor). The bottom detection system was mounted to the underneath of the MFP3D AFM plate. The two cantilever-sphere assemblies were put in a closed-fluid cell (Bioheater, Asylum Research, Oxford Instruments). With this setup, we conveniently exchange the solution in the fluid cell without disturbing the measuring system. The bottom cantilever was mounted at a slight angle (~5°) relative to the top cantilever to prevent possible laser cross-talk between the two probes. The two micro-spheres were then brought in close proximity of each other using a micrometer translation stage. Using the top view microscope of the MFP3D and monitoring the deflection signal of the two assemblies, we ensured that lateral offset between the spheres was minimal. The vertical separation between the spheres (D) was varied from a few nanometers to a few micrometers using the piezoelectric drive mechanism in the MFP3D. Both approach and retract force curves (see Figure 2) were examined to obtain accurate separation D: at contact (zero interparticle separation), the force-separation curve shows a vertical line. From Figure 1, it can be seen that D can be determined from

$$D = c - c_0 + x_1 - x_2, \tag{10}$$

where c is the displacement of the piezoelectric crystal and c_0 is a constant determined from the steep increase in force when the spheres touch.[29]

Two different measurements were performed: a slow measurement of deflections while varying the separation, and a fast measurement at a constant separation. The slow measurement (~1 kHz) was used to capture the force–separation curve[29] with a typical approach velocity of 1 μm/s (see Figure 2). Figure 2 shows that, during the slow measurement at varying separation, the force on approach is the same as the force when the spheres are pulled apart. This means that the lubrication

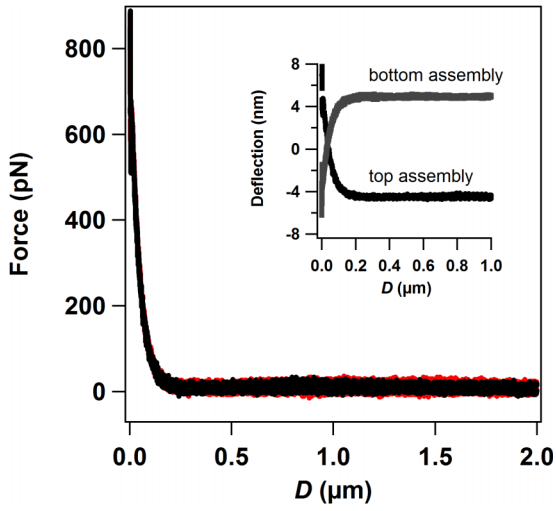

FIG. 2. Approach and retract force–separation curves obtained by driving the top cantilever-sphere assembly at 1000 nm s^{-1} toward, and then away from the bottom assembly. The overlay of the approach and retract curves shows that the lubrication force is very small compared to time-independent forces such as the double-layer forces. The inset shows that the measured deflection of the top and bottom assemblies is approximately equal and opposite. Results are for experiments in water and $a = 15\ \mu$m.

force at this approach velocity is much smaller than the quasi-static forces. The force is roughly exponential with separation and is consistent with the existence of a double-layer repulsion[29] that extends up to 150 nm from contact. We measured the force as a function of piezo velocity and found that the lubrication force was negligible compared to the double-layer force in the range of 10 nm/s to 1000 nm/s. The inset of Figure 2 shows that the deflection of one cantilever is approximately equal and opposite to the other assembly. We always choose two cantilevers with nearly matching spring constants, which means that the forces are nearly equal and opposite. Agreement with Newton's second law is consistent with correct calibration of the cantilever deflection.

The fast measurement (1 MHz) is used to measure the thermal fluctuations of the two cantilevers, and from there, to determine the cross-correlation in motion of the spheres. Here, the assemblies were held at a fixed separation for 16 s while the time series of the deflection of each assembly were collected using a high frequency data acquisition card (NI PCI-6110, National Instrument, Irvine, CA). Within each assembly, the AFM cantilever applies an external harmonic potential with a stiffness of 0.08 N m^{-1} on each sphere. This stiffness was measured in a separate experiment in air using the thermal method[30] and only pairs of cantilevers where the spring constant differed by less than 15% were utilized because our analysis assumes that the spring constants are the same. In our experiment, $\omega_0 = 25\ 000$ rad s^{-1} and $\upsilon = 10^{-6}$ m^2 s^{-1}. This results in $\mathrm{Re}_\omega = 6$ for a single particle, and $\mathrm{Re} \cong 10^{-4}$.

Analysis

We used a Langevin theoretical framework to quantify our results. The time dependent position of the spheres is given by

$$\begin{pmatrix} m\ddot{x}_1 \\ m\ddot{x}_2 \end{pmatrix} + \begin{pmatrix} \zeta_{11} & \zeta_{12} \\ \zeta_{21} & \zeta_{22} \end{pmatrix} \begin{pmatrix} \dot{x}_1 \\ \dot{x}_2 \end{pmatrix} + \begin{pmatrix} kx_1 \\ kx_2 \end{pmatrix} = \begin{pmatrix} f_1(t) \\ f_2(t) \end{pmatrix}, \tag{11}$$

where $m = k/\omega_0^2 = 120$ ng is the fluid loaded mass, and ζ_{ij} is the friction tensor: ζ_{ii} is the friction associated with the motion of a single particle, whereas $\zeta_{ij,i\neq j}$ is the friction that depends on the mutual (cross-correlated) motion of the two particles. For axisymmetric motion of two identical spheres, the friction tensor is symmetric with equal diagonal elements. $f_i(t)$ is the random

Brownian force with two moments[12]

$$\langle f_i(t)\rangle = 0 \tag{12}$$

and

$$\langle f_i(t)\, f_j(t')\rangle = 2\zeta_{ij} k_B T \delta(t-t'). \tag{13}$$

Equation (11) can be expressed in terms of a symmetric coordinate, $X_s = \frac{1}{\sqrt{2}}(x_1 + x_2)$, and an asymmetric coordinate, $X_{as} = \frac{1}{\sqrt{2}}(x_1 - x_2)$. The symmetric coordinate represents the motion of the center of mass of the two spheres (collective motion) and the asymmetric coordinate represents the differential motion of the two spheres (relative motion) (Figure 1). These coordinates are orthogonal and independent, i.e., $\langle X_s(t)\, X_{as}(0)\rangle = 0$. In terms of the new coordinates, Eq. (11) becomes

$$m\ddot{X}_s + \zeta_s \dot{X}_s + kX_s = f_s \tag{14}$$

and

$$m\ddot{X}_{as} + \zeta_{as}\dot{X}_{as} + kX_{as} = f_{as}, \tag{15}$$

where ζ_s and ζ_{as} are the friction coefficients in the symmetric and asymmetric coordinates, respectively. Similarly, f_s and f_{as} are the random Brownian forces sensed by the dual cantilever-sphere system in the symmetric and asymmetric coordinates, respectively. The noise spectra of the symmetric and asymmetric coordinates are $G_s = 4\int_0^\infty \langle X_s^2(t)\rangle \cos(\omega t)\, dt$ and $G_{as} = 4\int_0^\infty \langle X_{as}^2(t)\rangle \cos(\omega t)\, dt$ which from fluctuation-dissipation theorem are[15]

$$G_s = \frac{4k_B T\zeta_s}{(m\omega^2 - k)^2 + \zeta_s^2\omega^2}, \tag{16}$$

and

$$G_{as} = \frac{4k_B T\zeta_{as}}{(m\omega^2 - k)^2 + \zeta_{as}^2\omega^2}, \tag{17}$$

respectively. It is noted that from Eqs. (16) and (17), $G_{ij} = 4\int_0^\infty \langle x_i(t)\, x_j(0)\rangle \cos(\omega t)\, dt$ which for $i = j$ gives the self- (autocorrelation) noise spectrum of each assembly and for $i \neq j$ gives the mutual (cross-correlation) noise spectrum

$$G_{11} = \frac{(G_s + G_{as})}{2}; \quad G_{12} = \frac{(G_s - G_{as})}{2}. \tag{18}$$

In Eqs. (16) and (17), all the parameters are known prior to the correlation measurement except ζ_s and ζ_{as}. These are obtained from the best fit of Eqs. (16) and (17) to experimentally generated G_s and G_{as}, respectively. Elements of the friction tensor (Eq. (11)) can be obtained via

$$\zeta_{11} = \frac{\zeta_s + \zeta_{as}}{2}; \quad \zeta_{12} = \frac{\zeta_s - \zeta_{as}}{2}. \tag{19}$$

The friction coefficients ζ_{11} and ζ_{12} contain contributions from the sphere and the cantilever. However, our interest is in the sphere contribution only, so we must separate the two effects. For ζ_{12}, the contribution from cantilever-cantilever hydrodynamic interactions is negligible because the cantilevers are far apart (at least $4a \sim 60$ μm): experiments with cantilevers that were two times wider showed that G_{12} is negligible between two cantilevers (without attached spheres) at cantilever-cantilever separations of ≥ 60 μm (data not shown). The other hydrodynamic contribution to ζ_{12} is due to one cantilever-sphere assembly and cantilever of the other sphere. The minimum separation between the objects in this case is $2a \sim 30$ μm. This contribution is also insignificant and can be approximated from the radial fluid velocity field around an oscillating cylinder (the cylinder is the approximate model for an oscillating cantilever[31,32]). At 30 μm separation, the fluid velocity drops to less than 20% of the cantilever velocity (for $\mathrm{Re}_\omega \cong 6$ and $\omega_0 \cong 25\,000$ rad s^{-1}). For the previous case (60 μm separation), the fluid velocity drops to less than 7% of the cantilever

velocity. Thus, the cross-correlation in thermal fluctuations of the two assemblies is dominated by sphere-sphere interactions and by the fluid spanning the gap between the two spheres.

Unlike ζ_{12}, the friction coefficient for the motion of a single particle, ζ_{11}, includes the effect of the cantilever, and we wish to subtract this contribution. We *assume* that the contributions from the sphere and cantilever are additive: this assumption is based on the fact that the rms amplitude of thermal fluctuations is very small ($A = 0.2$ nm at the resonance frequency) compared to the length scale of a single sphere ($a = 15$ μm) and a single cantilever ($w = 20$ μm, where w is the cantilever width). We estimate the cantilever contribution using the expression for friction of a rectangular beam in viscous fluid[15,31]

$$\zeta_{\text{rect}} = \left(\tfrac{\pi}{4} w^2 L_{\text{cant}} \rho_f \omega \Gamma''\right) \Omega, \tag{20}$$

where $L_{\text{cant}} = 200$ μm is the cantilever length, and Γ'' is the imaginary component of the hydrodynamic function Γ[15,31]

$$\Gamma = 1 + \frac{4iK_1\left(-i\sqrt{i\,\text{Re}_\omega}\right)}{\sqrt{i\,\text{Re}_\omega}\,K_0\left(-i\sqrt{i\,\text{Re}_\omega}\right)}, \tag{21}$$

where $i = \sqrt{-1}$, K_1 and K_0 are the Bessel functions, and $\Omega(\omega)$ is the correction factor for a rectangular geometry.[31] For $\Omega(\omega) = 1$, Eqs. (20) and (21) yield the friction of a cylinder of length L_{cant}.[31] Equations (20) and (21) have been successfully applied to model cantilever oscillations in viscous fluid in various experiments.[33] The friction on a single sphere is then $\zeta_{\text{sph}} = \zeta_{11} - \zeta_{\text{rect}}$. We checked the validity of this assumption (linearity) by comparing theoretical and experimental values of ζ_{sph} at high frequency number and at large separations where the theoretical value is known (Eq. (4)).[3] At infinite separation, the experimental $\zeta_{\text{sph}} = 0.81$ μkg s^{-1} was calculated by subtracting the cantilever contribution $\zeta_{\text{rect}} = 0.86$ μkg s^{-1} (calculated from Eqs. (20) and (21)) from the friction of the cantilever-sphere assembly $\zeta_{11} = 1.66$ μkg s^{-1}. There is only 7% difference between the theoretical prediction $\zeta_{\text{Stokes}} = 0.76$ μkg s^{-1} (calculated from Eq. (4)) and the experimental value $\zeta_{\text{sph}} = 0.81$ μkg s^{-1}. From this point, our interest is in the friction of the sphere, so for simplicity we use ζ_{11} to describe the friction of single-sphere motion, i.e., our measured value of ζ_{11} with the cantilever contribution subtracted. We denote that as described above, there is no significant contribution from the cantilevers in the measured values of ζ_{12}; that is no subtraction was applied to calculate the mutual (cross-correlation) friction of the two spheres.

RESULTS

The thermally stimulated deflections of two cantilevers each with a spherical particle attached were measured at varying separations between the spheres. The time series of the sum in deflections ($X_{\text{s}} = \frac{1}{\sqrt{2}}(x_1 + x_2)$) were used to calculate the power spectral density of symmetric (collective or center of mass) motion and the time series of the difference ($X_{\text{as}} = \frac{1}{\sqrt{2}}(x_1 - x_2)$) in deflections were used to calculate the spectral density of the asymmetric (relative or differential) motion as described in the section on Analysis (Figure 1). The results are shown in Figure 3. At infinite separation, G_{s} is very similar to G_{as} and they both approach G_{11} (the autocorrelation power spectral density). The symmetric motion is a weak function of separation: G_{s} increases very gradually as the separation decreases. In contrast, the asymmetric motion is a strong function of separation. Data for G_{s} and G_{as} were fitted with Eqs. (16) and (17) to obtain the values of ζ_{s} and ζ_{as}. The external potential is applied by the cantilever of constant stiffness, so we keep k the same at all separations. We assume also that m is independent of separation, so all the variation in G_{s} and G_{as} arises from ζ_{s} or ζ_{as}. The variation in ζ_{s} or ζ_{as} as a function of separation is shown in Figure 4. The abscissa on this graph is the dimensionless center-to-center distance, $\rho = r/a$. The slight increase in the amplitude of the symmetric spectral density is associated with the slight decrease in magnitude of the friction of symmetric motion (ζ_{s}). In keeping with the previous interpretation,[17] we interpret this decrease in friction as an increase in the tendency of the fluid flow generated by one sphere to entrain the neighboring sphere when the spheres are closer to each other. The spectrum for G_{as} is similar to a spectrum for an increasingly damped oscillator as the separation decreases. Fitted values for ζ_{as}

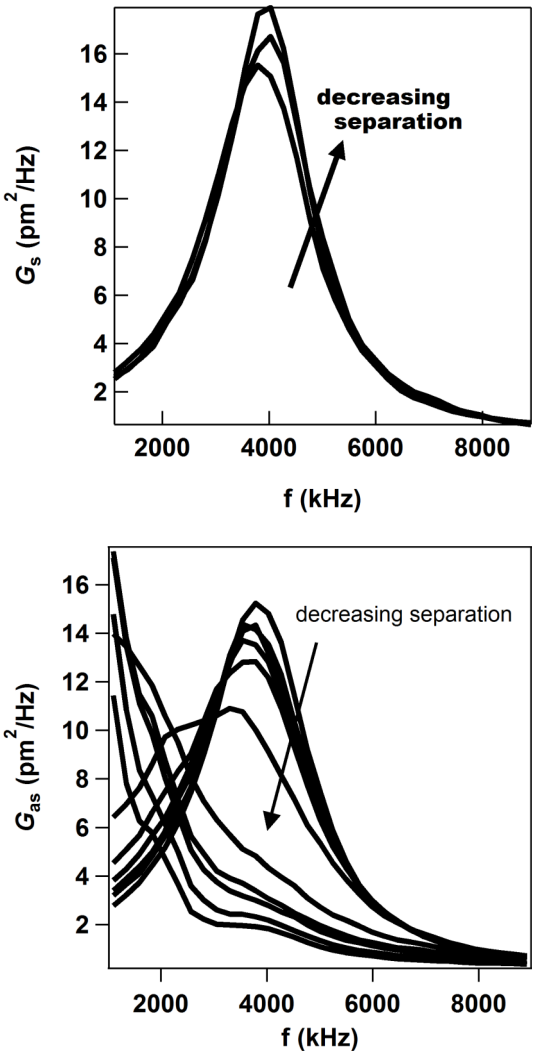

FIG. 3. Power spectral density of the symmetric motion, G_s, and power spectral density of the asymmetric motion, G_{as}, at varying separations D. Only three separations are shown in the top graph, $D = \infty$, 4 μm, and 10 nm. Decreasing separations in the bottom graph are $D = \infty$, 14 μm, 11 μm, 7 μm, 4 μm, 2 μm, 400 nm, 150 nm, 100 nm, 30 nm, and 10 nm. Results are for experiments in water and $a = 15$ μm.

(Figure 4) quantitatively show the increasing damping at smaller separations. The increase in the friction of the asymmetric motion (ζ_{as}) at closer separations reflects the difficulty of squeezing the fluid into, and out of, the gap between the two spheres.

G_{12} is calculated from the difference between G_s and G_{as} (Eq. (18)) and is approximately zero at large separation (indicating that the particle motions are uncorrelated) and increases in magnitude with smaller separation (indicating that the particle motions are highly correlated) (see Figure 5). The solid lines in Figure 5 are plots of G_{12} calculated from Eq. (18) using G_s (ζ_s) and G_{as} (ζ_{as}) obtained from the fits to the respective experimental power spectra (Figure 3) using Eqs. (16) and (17). The trend of G_{12} is consistent with the trends of G_s and G_{as} : the increase in fluid coupling at smaller separations dampens the asymmetric motion and enhances the symmetric motion (Figure 3).

A comparison to theoretical predictions of the friction coefficients is facilitated by normalizing the measured friction coefficient by the Stokes' drag, $6\pi\eta a$, as shown in Figure 6. Normalized data are signified by ζ^*_{11} and ζ^*_{12}. The only high frequency number equation that we have is for ζ^*_{11} for a *free* sphere (Eq. (4)). From Figure 6, we see that our data agree with this prediction within only 7% difference, which is less than the systematic error in our experiment due to uncertainty in the spring

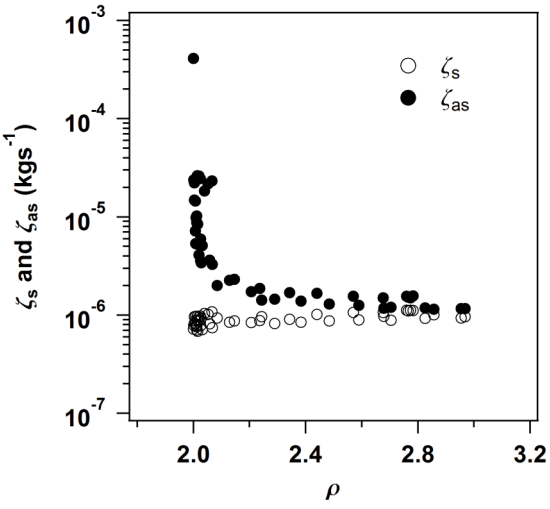

FIG. 4. Values of ζ_s and ζ_{as} obtained from fits to Eqs. (16) and (17) using experimental G_s and G_{as}. Data are plotted as a function of the dimensionless separation ($\rho = r/a$). Results are for experiments in water and $a = 15\ \mu$m.

constant and sphere radius. Hinch and Nitsche[9] presented a theory for the interparticle hydrodynamic interaction that applies at high frequency number and small separation, but the numerical values for the friction coefficients are not available in their paper. We compare our results to the theory for steady interparticle flow. For gap width much larger than the particle radius, Jeffrey and Onishi give the following asymptotic expressions:[6]

$$\zeta_{11}^{*} = 1 + \frac{9}{4\rho^2} + \frac{93}{16\rho^4} + \frac{1197}{64\rho^6} \tag{22}$$

$$-1 \times \zeta_{12}^{*} = \frac{3}{2\rho} + \frac{19}{8\rho^3} + \frac{387}{32\rho^5}. \tag{23}$$

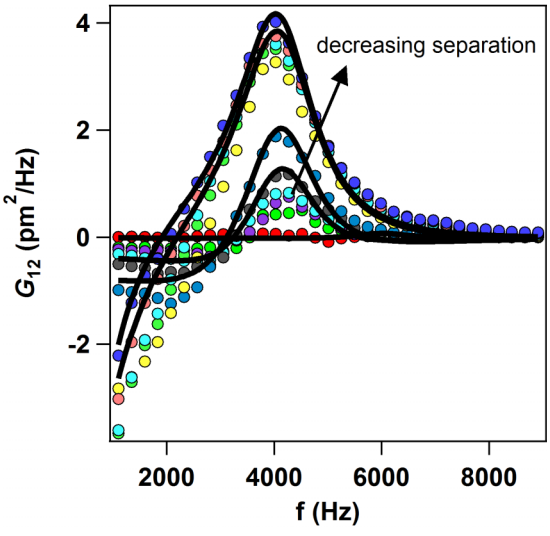

FIG. 5. Cross-correlation spectral density, G_{12}, at varying separations D. Decreasing separations are $D = \infty$, 14 μm, 11 μm, 7 μm, 4 μm, 2 μm, 400 nm, 150 nm, 100 nm, 30 nm, and 10 nm. Solid lines show the quality of fits for separations $D = \infty$, 4 μm, 2 μm, 30 nm, and 10 nm. At any given frequency, the magnitude of G_{12} changes monotonically with separation. Results are for experiments in water and $a = 15\ \mu$m.

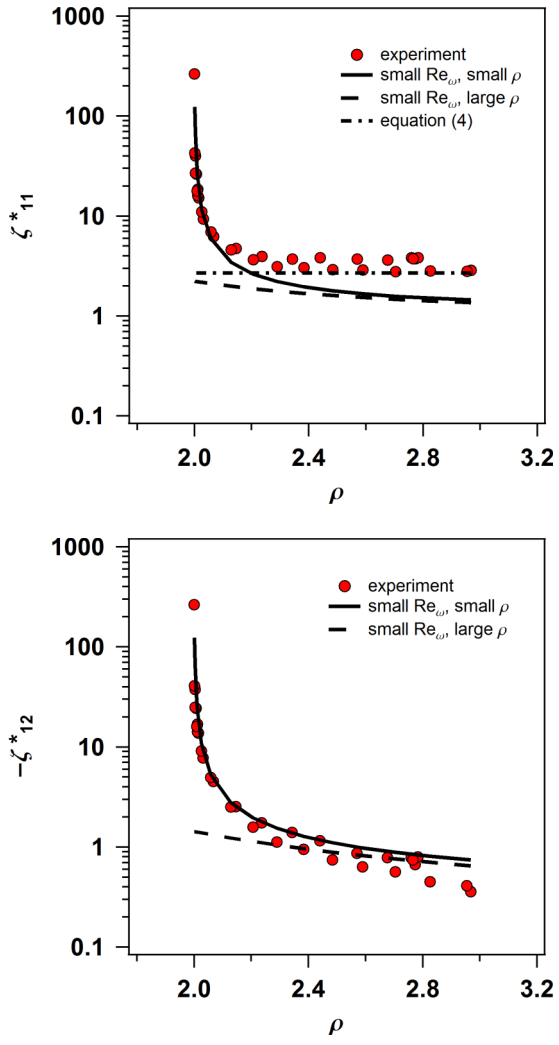

FIG. 6. Friction of single sphere ζ^*_{11}, and friction of cross-correlated motions of two spheres, ζ^*_{12}, as a function of dimensionless separation, $\rho = r/a$. Data are normalized by $6\pi\eta a$ and we plotted $-\zeta^*_{12}$. Experimental data are compared with Eqs. (22) and (23) (small Re_ω and large ρ) and with Eqs. (24) and (25) (small Re_ω and small ρ).[6] Equation (4) is the high frequency number friction on a free sphere. Results are for experiments in water and $a = 15\ \mu$m.

These equations are plotted in Figure 6 and clearly do not fit the data well. They fail at small separations as expected for a large separation approximation. At large separation, Eq. (22) fails to predict ζ^*_{11}, but the value of ζ^*_{12} is reasonably accurate. We will return to the agreement between theoretical and experimental values of ζ^*_{12} later. For two spheres that are nearly touching, Jeffrey gives the following asymptotic expressions (also from Ref. 6):

$$\zeta^*_{11} = \frac{1}{4(\rho-2)} - \frac{9}{40}\ln(\rho-2) + 0.99536 - \frac{3(\rho-2)}{112}\ln(\rho-2) + 0.19(\rho-2) \tag{24}$$

$$-1\times\zeta^*_{12} = \frac{1}{4(\rho-2)} - \frac{9}{40}\ln(\rho-2) + 0.35022 - \frac{3(\rho-2)}{112}\ln(\rho-2) + 0.13185(\rho-2)\,. \tag{25}$$

As shown in Figure 6, these expressions agree with our data for ζ^*_{11} and ζ^*_{12} at small separations despite the fact that they are steady single-particle and interparticle flow predictions and $Re_\omega = 6$ for a single particle in our experiments. Our explanation for the observed agreement between data at high frequency number and theory at low frequency number is that ζ^*_{12} is dominated by flow

in the thin film between the spheres. Our data show that for interparticle gap width shorter than twice the penetration depth δ_s, the interparticle flow is steady and thus the propagation of stress in the thin fluid film is effectively instantaneous despite the high frequency of a single particle oscillation. In Figure 6, $\delta_s = 9$ μm at the resonance frequency, so $2\delta_s$ corresponds to $\rho = 3.2$. As shown in Figure 6, Jeffrey's Eq. (25) provides a reasonable fit to the measured data from contact out to $\rho = 3.2$, justifying the choice of separations less than $2\delta_s$ as the range for neglecting fluid inertia. The quantitative agreement between Eq. (23) and the experimental ζ_{12}^* at large separations (but still overlapping Stokes layers, $D < 2\delta_s$) is for the same reason.

The agreement between Jeffrey's theory and our measurements would be more satisfying if confirmed at a second (high) frequency. It is difficult to vary the frequency in our experiment, but by the addition of a heavier mass in the form of a larger sphere (100 μm-diameter) to the cantilever, we are able to shift the resonance frequency down to 1 kHz. A comparison of the cross-correlation friction ζ_{12} as a function of separation at the two frequencies is shown in Figure 7. ζ_{12} and r are shown normalized to the radius of the particle a to account for the different sphere radii (see Eq. (25)). After appropriate normalization, the cross-correlation friction shows no effect of frequency when the Stokes layers of the two particles overlap.

As described in the Introduction, we account for the experimental observation that the effects of fluid inertia do not appear to be important at small separations by introducing the characteristic length $D/2$ in calculation of $\mathrm{Re}_{\omega,g}$ (the frequency number for fluid flow in the gap width) giving $\mathrm{Re}_{\omega,g} = \frac{1}{2}D^2/\delta_s^2$ where the effect of the fluid density, viscosity, and the frequency of oscillation is included in δ_s. This definition implies that at a fixed frequency of oscillation, the contribution of fluid inertia grows as the gap between the particles grows and for a fixed interparticle separation, the fluid inertia becomes more important at a higher frequency of oscillation. The properties of the fluid, in which the particles are dispersed, are also important: the lower the fluid kinematic viscosity the higher the inertial response. So, for example, the inertial response of water is higher than for air between two colloidal particles. Using the above definition, all the experimental data presented here are at $\mathrm{Re}_{\omega,g} = \frac{1}{2}D^2/\delta_s^2 < 1$.

The fact that the coupling of two spheres oscillating at high frequency (4 kHz) can be treated as a low frequency number problem for a simple fluid (water) suggests that the apparatus and the method of analysis of thermal oscillations described in this paper could be used for studying the hydrodynamic drag on two colliding particles, a problem that is important in the study of colloidal and nanoparticle suspensions. As an example, here, we briefly use the technique to examine the

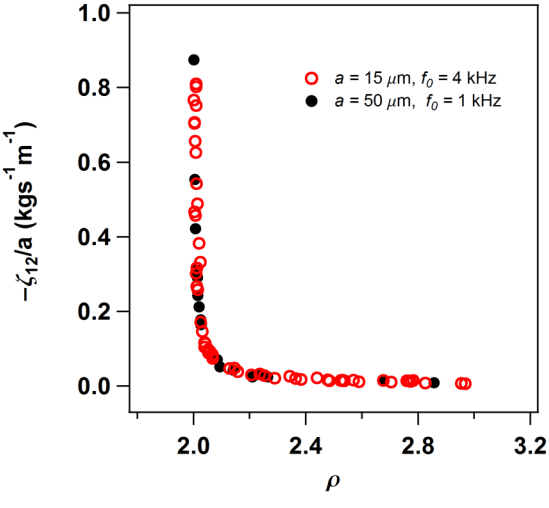

FIG. 7. Effect of resonance frequency f_0 on ζ_{12}. The friction of cross-correlated motions of two spheres normalized to the radius of the particle a is shown as a function of dimensionless separation $\rho = r/a$ for two frequencies, 4 and 1 kHz. The lower frequency was obtained by using larger particles, $a = 50$ μm, than in the other experiments in this paper where $a = 15$ μm. Results are for experiments in water.

effect of nanoparticles on the hydrodynamic interaction between micron-sized particles in water. It has been well known since the time of Einstein that colloidal particles increase the viscosity of solutions according to the volume fraction of the suspension[34]

$$\eta = \eta_0 (1 + 2.5\phi), \tag{26}$$

where η_0 is the viscosity of the base fluid and ϕ is the volume fraction of particles in suspension.

Recently, Bhattacharya and Blawzdziewicz[35] postulated that the hydrodynamic force on a micrometer-size particle approaching a wall in a nanoparticle solution would behave as if the viscosity of the intervening fluid would gradually trend toward the pure solvent viscosity at smaller separations. The reduction in viscosity should arise because of exclusion of the nanoparticles from the gap width. Using measurements in which a sphere was driven toward a plate, James and Walz[36] confirmed this trend: the fitted viscosity diminished with diminishing separation between the particle and wall. The remarkable feature of these measurements is that viscosity was measurably reduced up to 100 times the hard sphere diameter of the nanoparticles (~2 μm), meaning that the change in viscosity affects much of the important range for interparticle collisions.[36]

Here, we determine the viscosity from measurement of the coupling between two particles when they were driven by thermal noise using the method described earlier in this paper and from the following equation (see Jeffrey's Eq. (25)):

$$\eta = \frac{1}{6\pi a}\left[\frac{1}{4(\rho-2)} - \frac{9}{40}\ln(\rho-2) + 0.350\,22 - \frac{3(\rho-2)}{112}\ln(\rho-2) + 0.13185(\rho-2)\right]^{-1}\zeta_{12}. \tag{27}$$

The viscosity data as a function of separation are shown in Figure 8. Figure 8 shows the same trend as the measurement of James and Walz.[36] The difference between data here and results of James and Walz (comparison not shown) is likely due to differences in the volume fraction of the particles and the ionic strength of solution, to which the viscosity is quite sensitive. This application shows the usefulness of the measurement of the thermal motions for determining fluid properties.

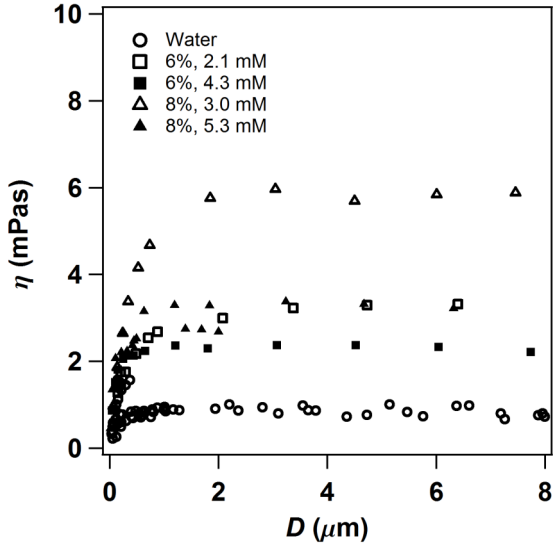

FIG. 8. Viscosity of nanoparticle suspension in thin film between two colloidal particles, determined from Eq. (27). The symbols correspond to (○) water, (□) 6% and 2.1 mM, (■) 6% and 4.3 mM, (△) 8% and 3 mM, and (▲) 8% and 5.3 mM. The data show that the viscosity of suspensions starts to decrease at about 2 μm gap width that is about 100 times the hard sphere diameter of silica particles (22 nm). At the smallest separations, the viscosity of suspensions approaches the viscosity of base fluid, water.

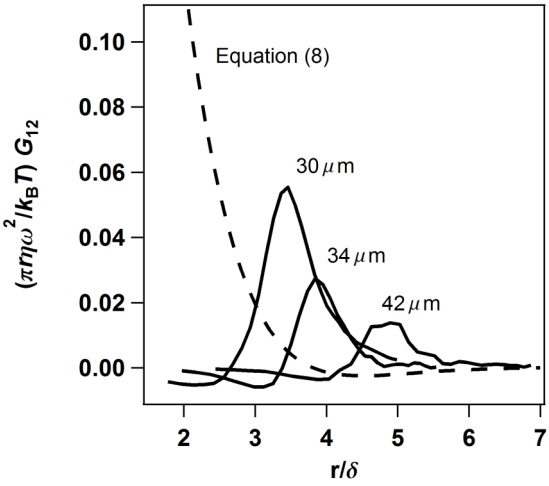

FIG. 9. Normalized cross-correlation spectral density $(\pi r\eta\omega^2/k_BT)G_{12}$ compared for several separations with the theoretical expression $(e^{-z}/z^2)[(1+z)\sin(z)-z\cos(z)]$ in Eq. (8) and plotted versus the dimensionless ratio $z=r/\delta$. The discrepancy between our experimental data and Eq. (8) arises because the particle in the experiment has significant inertial and restoring forces compared to the viscous drag force. For each experimental data set, r and υ are fixed, so r/δ is a function of frequency only. Results are for experiments in water and $a=15$ μm.

DISCUSSION

Comparison to optical tweezers experiments

Equation (6) assumes that the particle's inertial and restoring forces are insignificant when compared with the viscous drag force (i.e., a highly overdamped oscillator) and therefore is applicable for analysis of optical tweezers experiments. In contrast, the particle's inertial and restoring forces are important in the two cantilever-sphere experiment, and thus Eq. (6) is inapplicable. Figure 9 shows that Eq. (6) fails to predict the interparticle hydrodynamic response in our experiments. Thus, the particle inertial and restoring forces cannot always be ignored when discussing hydrodynamic interactions between particles.

Comparison to conventional drainage experiments

A conventional drainage experiment is often used to obtain the lubrication force and thus the friction coefficient acting on a sphere approaching another fixed object such as a plate or sphere.[37,38] In such experiments, the fluctuations in the deflection of the AFM cantilever are usually low-pass filtered, and thus the fast fluctuations and time-dependent effects are excluded.[15,31] Two of the major weaknesses of such an approach are avoided in the experiments described here. First, the conventional drainage experiment measures the sum of the quasistatic force and the lubrication

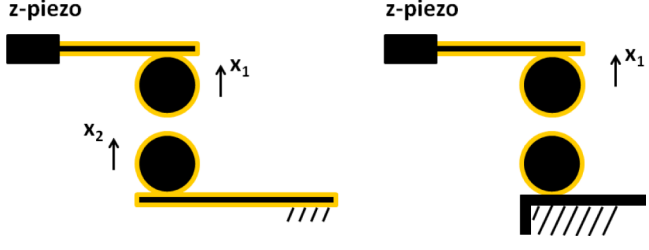

FIG. 10. The current experiment reduces the hydrodynamic coupling between cantilevers by keeping them well separated and antiparallel (left). A conventional drainage experiment could achieve a similar effect by attaching the bottom sphere to a step edge (right).

force, sometimes making it difficult to resolve the lubrication force. For example, the quasistatic double-layer force in Figure 2 completely obscures the lubrication force, whereas the lubrication force can be easily separated and resolved as shown here from the analysis of the Brownian motion. Second, the conventional drainage experiment suffers from significant interfering hydrodynamic contributions due to the interaction between the cantilever and the bottom plate. This problem is largely solved in this work by supporting the bottom sphere on a cantilever that is small and antiparallel to the top cantilever such that the coupling between opposing cantilevers is weak. This type of improvement could also be made to the conventional drainage experiment, for example, by attaching the lower sphere to the edge of a step (Figure 10).

CONCLUSIONS

We have presented a direct measurement of the hydrodynamic interactions between two microspheres for the conditions of low Reynolds number and high single-particle frequency number (at resonance frequency 4 kHz). At small separations, the friction of the asymmetric motion increases dramatically because of the extra difficulty in squeezing the liquid out of a small film. In contrast, the friction of the symmetric motion decreases slightly because each particle is dragged in the wake of the other particle.

At small separations between the spheres ($D < 2\delta_s$), the measured value of the interparticle friction is well predicted by *low frequency number* theory (Jeffry's expression from Ref. 6). This suggests that we use a frequency number for the interparticle hydrodynamic interaction that includes an explicit dependence on the separation of the spheres, for example, $\mathrm{Re}_{\omega,g} = \frac{1}{2}D^2/\delta_s^2$. From this definition, inertial effects should be included for $\mathrm{Re}_{\omega,g} > 1 \Rightarrow D/\delta_s > 1.4$. The physical interpretation of this relation is that when the separation between the spheres is less than about two times the wake of the unsteady viscous boundary layer, then the flow is effectively a Stokes' flow. This is because in narrow gaps, frictional forces dominate fluid inertial effects. As the separation D increases, the low frequency number does not accurately describe the experiment, particularly for the friction of single particle motion. This is explained as a diminishing effect of confinement of the liquid between particles. The behavior of the particle at large separation asymptotes to a magnitude that is close to the prediction by Stokes for a single particle at high frequency number. Our work is only over a narrow range of frequencies, future work over a wider range of frequencies could determine whether the hydrodynamic coupling between two spheres always approximates low frequency number behavior in close proximity.

ACKNOWLEDGMENTS

The authors would like to thank John Walz, Jason Karcz, Shunxi Ji, and David Herman. The work described in this paper was funded by the National Science Foundation via Award No. CBET-0959228.

[1] G. G. Stokes, "On the effect of the internal friction of fluids on the motion of pendulums," Cambridge Philos. Soc. Trans. **IX** (1851), 8-106.
[2] P. Mazur and D. Bedeaux, "A generalization of Faxén's theorem to nonsteady motion of a sphere through an incompressible fluid in arbitrary flow," Physica **76**(2), 235-246 (1974).
[3] L. D. Landau and E. M. Lifshitz, *Fluid Mechanics* (Pergamon Press, New York, 1987).
[4] D. Bedeaux and P. Mazur, "Brownian motion and fluctuating hydrodynamics," Physica **76**(2), 247-258 (1974).
[5] D. J. Jeffrey, "Low-Reynolds-number flow between converging spheres," Mathematika **29**(01), 58-66 (1982).
[6] D. J. Jeffrey and Y. Onishi, "Calculation of the resistance and mobility functions for two unequal rigid spheres in low-Reynolds-number flow," J. Fluid Mech. **139**, 261-290 (1984).
[7] S. S. Tabakova and Z. D. Zapryanov, "On the hydrodynamic interaction of two spheres oscillating in a viscous fluid.—I. Axisymmetrical case," J. Appl. Math. Phys. **33**(3), 344-357 (1982).
[8] S. S. Tabakova and Z. D. Zapryanov, "On the hydrodynamic interaction of two spheres oscillating in a viscous fluid. II. Three dimensional case," J. Appl. Math. Phys. **33**(4), 487-502 (1982).
[9] E. J. Hinch and L. C. Nitsche, "Nonlinear drift interactions between fluctuating colloidal particles: Oscillatory and stochastic motions," J. Fluid Mech. **256**, 343-401 (1993).
[10] M. Atakhorrami, G. H. Koenderink, C. F. Schmidt, and F. C. MacKintosh, "Short-time inertial response of viscoelastic fluids: Observation of vortex propagation," Phys. Rev. Lett. **95**, 208302 (2005).

[11] M. Atakhorrami, D. Mizuno, G. H. Koenderink, T. B. Liverpool, F. C. MacKintosh, and C. F. Schmidt, "Short-time inertial response of viscoelastic fluids measured with Brownian motion and with active probes," Phys. Rev. E **77**, 061508 (2008).
[12] J. C. Meiners and S. R. Quake, "Direct measurement of hydrodynamic cross correlations between two particles in an external potential," Phys. Rev. Lett. **82**(10), 2211-2214 (1999).
[13] R. J. Hunter, "Recent developments in the electroacoustic characterisation of colloidal suspensions and emulsions," Colloids Surf., A **141**(1), 37-66 (1998).
[14] B. Lukic, S. Jeney, C. Tischer, A. J. Kulik, L. Forro, and E. L. Florin, "Direct observation of nondiffusive motion of a Brownian particle," Phys. Rev. Lett. **95**, 160601 (2005).
[15] M. R. Paul, M. T. Clark, and M. C. Cross, "The stochastic dynamics of micron and nanoscale elastic cantilevers in fluid: Fluctuations from dissipation," Nanotechnology **17**(17), 4502-4513 (2006).
[16] W. M. Deen, *Analysis of Transport Phenomena* (Oxford University Press, New York, 1998).
[17] S. Henderson, S. Mitchell, and P. Bartlett, "Direct measurements of colloidal friction coefficients," Phys. Rev. E **64**, 061403 (2001).
[18] P. Bartlett, S. I. Henderson, and S. J. Mitchell, "Measurement of the hydrodynamic forces between two polymer–coated spheres," Philos. Trans. R. Soc., A **359**(1782), 883-893 (2001).
[19] J. C. Crocker, "Measurement of the hydrodynamic corrections to the Brownian motion of two colloidal spheres," J. Chem. Phys. **106**(7), 2837-2840 (1997).
[20] M. Reichert and H. Stark, "Hydrodynamic coupling of two rotating spheres trapped in harmonic potentials," Phys. Rev. E **69**, 031407 (2004).
[21] E. R. Dufresne, T. M. Squires, M. P. Brenner, and D. G. Grier, "Hydrodynamic coupling of two Brownian spheres to a planar surface," Phys. Rev. Lett. **85**(15), 3317-3320 (2000).
[22] T. M. Squires and T. G. Mason, "Fluid mechanics of microrheology," Annu. Rev. Fluid Mech. **42**, 413-438 (2010).
[23] T. B. Liverpool and F. C. MacKintosh, "Inertial effects in the response of viscous and viscoelastic fluids," Phys. Rev. Lett. **95**, 208303 (2005).
[24] M. Radiom, C. D. F. Honig, J. Y. Walz, M. R. Paul, and W. A. Ducker, "A correlation force spectrometer for single molecule measurements under tensile load," J. Appl. Phys. **113**, 013503 (2013).
[25] M. Radiom, B. Robbins, C. D. F. Honig, J. Y. Walz, M. R. Paul, and W. A. Ducker, "Rheology of fluids measured by correlation force spectroscopy," Rev. Sci. Instrum. **83**, 043908 (2012).
[26] C. D. F. Honig, M. Radiom, B. A. Robbins, J. Y. Walz, M. R. Paul, and W. A. Ducker, "Correlations between the thermal vibrations of two cantilevers: Validation of deterministic analysis via the fluctuation-dissipation theorem," Appl. Phys. Lett. **100**, 053121 (2012).
[27] J. E. Sader, *Atomic Force Microscopy: Cantilever Calibration*, in Encyclopedia of Surface and Colloid Science, 2nd ed., edited by P. Somasundaran (CRC Press, 2006), Vol. 2, pp. 839-849.
[28] G. Meyer and N. M. Amer, "Novel optical approach to atomic force microscopy," Appl. Phys. Lett. **53**(12), 1045-1047 (1988).
[29] W. A. Ducker, T. J. Senden, and R. M. Pashley, "Measurement of forces in liquids using a force microscope," Langmuir **8**(7), 1831-1836 (1992).
[30] J. L. Hutter and J. Bechhoefer, "Calibration of atomic-force microscope tips," Rev. Sci. Instrum. **64**(7), 1868-1873 (1993).
[31] J. E. Sader, "Frequency response of cantilever beams immersed in viscous fluids with applications to the atomic force microscope," J. Appl. Phys. **84**(1), 64-76 (1998).
[32] M. R. Paul, M. T. Clark, and M. C. Cross, "Coupled motion of microscale and nanoscale elastic objects in a viscous fluid," Phys. Rev. E **88**(4), 043012 (2013).
[33] J. W. M. Chon, P. Mulvaney, and J. E. Sader, "Experimental validation of theoretical models for the frequency response of atomic force microscope cantilever beams immersed in fluids," J. Appl. Phys. **87**(8), 3978-3988 (2000).
[34] A. Einstein, "Eine neue bestimmung der moleküldimensionen," Ann. Phys. **324**(2), 289-306 (1906) [in German].
[35] S. Bhattacharya and J. Blawzdziewicz, "Effect of small particles on the near-wall dynamics of a large particle in a highly bidisperse colloidal solution," J. Chem. Phys. **128**, 214704 (2008).
[36] G. K. James and J. Y. Walz, "Hydrodynamic force on a microparticle approaching a wall in a nanoparticle dispersion: Observation of a separation-dependent effective viscosity," Langmuir **28**(1), 92-103 (2011).
[37] C. D. F. Honig and W. A. Ducker, "Squeeze film lubrication in silicone oil: Experimental test of the no-slip boundary condition at solid–liquid interfaces," J. Phys. Chem. C **112**(44), 17324-17330 (2008).
[38] C. D. F. Honig, J. E. Sader, P. Mulvaney, and W. A. Ducker, "Lubrication forces in air and accommodation coefficient measured by a thermal damping method using an atomic force microscope," Phys. Rev. E **81**, 056305 (2010).